Impurity density determination using charge exchange and beam emission spectroscopy at ASDEX Upgrade

R. Dux, B. Geiger, R. M. McDermott, T. Pütterich, E. Viezzer and ASDEX Upgrade team

Max-Planck-Institut für Plasmaphysik, EURATOM Association, Garching, Germany

Charge exchange recombination spectroscopy (CXRS) on the neutral heating beam is a well established method to measure impurity density profiles at ASDEX Upgrade. The *active* impurity emission is induced by charge exchange reactions between beam neutrals and impurity ions. The impurity density can be determined from the measured radiance provided the densities of the three neutral beam species (full, half and third energy components) along the line-of-sight are known. These neutral densities are not measured, but calculated with a beam attenuation code for a given species mix. Lately, the beam observation optics of one toroidal CXRS system has been refurbished and equipped with 3 rows of 30 fibres. At the observed 60 keV beam, the images of the 3 rows are vertically separated by only $\Delta Z \approx 1.6$ cm, which is small compared to the beam height of about 30 cm. This offers the possibility to measure CXRS and the D_α emission of the beam on virtually the same lines-of-sight and to cross-check the neutral beam density evaluation.

Experimental Setup

For the beam emission spectroscopy a conventional Czerny-Turner-spectrometer with a 1200 L/mm grating, 1 m focal length and f-number of 10 was upgraded with a telescope of two cylindrical quartz lenses behind the camera mirror. The first lens has f=-200 mm and is situated about 200 mm in front of the detector, while the second lens has f=150 mm and is located about 50 mm behind the first lense. By adjusting the distance of the lenses, the astigmatism of the Czerny-Turner setup can be compensated and allows the image of 15 fibres with a diameter of 400 μm to fit onto a 6.6×6.6 mm CCD detector while maintaining good spectral resolution. The lines-of-sight that belong to these fibres cover the plasma from the centre to the pedestal top. The complete system has been calibrated using an integrating sphere inside the torus as a standard for spectral radiance.

At λ=656.1 nm, the spectral resolution is $\Delta\lambda_{\text{FWHM}}$=0.039 nm and 0.071 nm for a width of the entrance slit of 50 μm (as used for the upper spectrum in Fig.1) and 100 μm (Fig.3). In both wings of the instrumental line profile, there are several minor peaks. The largest of these peaks is at ± 1 nm and reaches $\approx 1.2 \times 10^{-3}$ of the maximum signal. Reflections at the uncoated lens surfaces (R=3.5×10^{-2}) are held responsible for these peaks and might be cured by an anti-reflection coating. At present, the spectra for plasmas with large passive D_α radiation have an additional peak in the spectral region of the beam emission spectrum and reliable measurements can only be done for beam-blips, where the difference of the spectra after and before the switch-on of the beam is taken for further analysis. The measured spectra are fitted by a function that contains a model for the beam emission spectrum of each energy component and the beam halo.
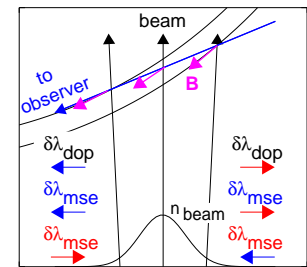
Beam Emission Spectrum

The model for the beam emission spectrum calculates line splitting and line strength due to the motional Stark effect (the Paschen-Back effect is neglected), the Doppler-shift and the Doppler-broadening due to the velocity distribution of the beam. The velocity distribution of the beam is calculated according to the following model. The beam atoms start from two vertically stacked rectangular grids with height h =0.25 m and width w =0.22 m. Each point on a

grid emits the same number of atoms per second. The mean starting velocity is directed to a horizontal and vertical focus which is at a distance f_h=6.5 m and f_v=8.5 m from the grid. The two grids are vertically inclined against each other by an angle α=0.97^0, such that the focus of both the upper and lower plate is at about the same vertical position. The velocity direction has an angular spread which is described by a Gaussian distribution with 1/e-width γ. This width is equal for both directions but varies slightly for the three energy components of the beam, i.e. γ=0.83^0, 0.87^0 and 1.0^0 for the full, half and third energy component. The values for f_h, α and γ have been determined during beam injections into the gas filled torus without magnetic field, such that the pure Doppler spectra could be measured on many toroidal and poloidal lines-of-sight. The toroidal lines-of-sight have an angle $\beta \approx 7.3^0$ with respect to the horizontal beam direction and give information about the horizontal velocity distribution, while the poloidal CXRS system with $\beta \approx 97^0$ is mostly sensitive to the vertical distribution. A comparison of the measured spectra (crosses) and the beam model (lines) is shown in Fig.1 for one toroidal and one poloidal sightline. For the toroidal observation, the angle between the direction of the beam centre and the sightline φ is larger (φ=111.6^0 compared to 99.5^0), such that the line shift $\Delta\lambda_{dop} = \lambda_0 v \cos\varphi / c$ is increased, hence, leading to a better separation of the spectra of the three energy components. For the poloidal sightline, the fitted lines are asymmetric due to an assumed imbalance of 10% for the emission from the two grids. The total line strength of each component is a free fit parameter since it is not based on an excitation model of the beam atoms in the gas target. The measured line strengths are constant throughout the whole observed part of the beam path. Thus, the beam emission was used to perform a relative calibration of the CXRS and beam emission spectrometers.
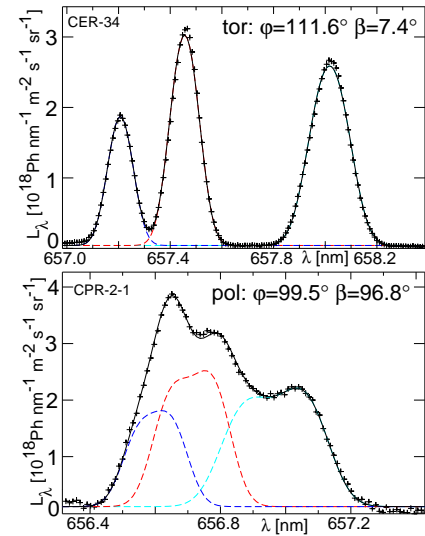
Fig.1: *Beam emission spectra without magnetic field for a poloidal and a toroidal chord: The crosses are the data, the dashed lines are the fits for each energy component with the black line as the total of all components.*

For the line splitting with magnetic field, we consider the pure motional Stark effect (MSE). It produces a symmetric multiplet of 15 lines, where the very weak 6 outermost lines are neglected. The line shift is $\Delta\lambda_{mse}$[nm]= $2.76\times10^{-8}kE$[V/m] with k=-4,-3,...,4 and $E = |\vec{v} \times \vec{B}|$. The line strength of each component is calculated assuming statistical equilibrium. The MSE spectrum is obtained by calculating the velocity distribution of the beam atoms for each point on the sightline, projecting the distribution onto the corresponding wavelength shift due to Doppler effect and MSE and by integrating the result along the sightline. For each energy component of the beam, this creates an asymmetric MSE feature as can be seen in Fig.3. The asymmetry can be explained with the sketch shown in Fig.2. The black arrows denote the average velocity direction of the beam atoms, while the roughly Gaussian curve at the bottom gives the beam density. The blue arrow indicates the line-of-sight to the observer. Fur-

Fig.2: *The large beam diameter causes an asymmetry in the MSE spectrum (see text).*

thermore, the B-field vectors in magenta are shown together with two flux surfaces. On the left side of the beam, the B-field is stronger and more perpendicular to the beam velocity compared

to the right side. The $\delta\lambda$ arrows indicate the relative wavelength shift with respect to the line shift at the center of the beam. The Doppler effect causes a relative blue/red shift at the left/right side. For the blue shifted lines of the MSE multiplet, the relative shifts have the same direction, while for the red shifted part of the multiplet, the relative shifts are reversed. Thus, the line broadening due to Doppler effect and MSE add up for the blue shifted lines and partly cancel each other for the red shifted lines. The effect is strongest for the central lines-of-sight and for the outermost π-lines, where the ratio of the line maxima reaches 1.65.

The line strength varies with the angle ψ between $\vec{E}$ and the direction $\vec{k}$ of the emitted radiation: for the 3 innermost σ-lines $L_\sigma \propto 1 + \cos^2\psi$ and for the remaining π-lines $L_\pi \propto 1 - \cos^2\psi$. Before reaching the objective the light is reflected by a Rhodium mirror with a nominal index of refraction $n = 2.21 + i5.79$ at 656 nm. For the used sightlines, the angle of incidence is in the range of 56.4^0-67.1^0 and there is a considerably lower reflection coefficient for p- than for s-polarised light, i.e. R_p/R_s=0.64-0.76. The direction of the s-polarisation $\vec{e}_s$ is perpendicular to the mirror normal $\vec{n}$ and to $\vec{k}$. With the angle ϕ between $\vec{e}_s$ and the $\vec{k}$-$\vec{E}$ plane, the measured line strengths are: $L_\sigma \propto R_p + R_s\cos^2\psi + (R_s - R_p)\sin^2\psi\sin^2\phi$ and $L_\pi \propto R_s\sin^2\psi\cos^2\phi + R_p\sin^2\psi\sin^2\phi$.

The shape of the MSE spectrum is thus fixed and only the line strength due to the three energy components of the beam are free parameters in the fit function. An integral part of the beam emission spectrum is the broad line due to the beam halo, whose radiance is a few times stronger than the MSE features. The halo emission is unpolarised and well described by a shifted Gaussian. At present, we either use T_i and v_{rot} from the CXRS diagnostic to define the line shape or leave it together with the radiance of the halo as free parameters in the fit. Finally, the spectrum is folded with the instrumental line shape and a constant background is the last fit parameter. At present, we neglect the FIDA emission in the model function.

Fig.3 shows two measured spectra for the innermost line-of-sight and the according fit to the data. The data were obtained from beam blips into a hot, low density (#26426) and a high density discharge(#27066). The difference of the spectral radiances can not be evaluated around the passive D_α line, where the camera is strongly saturated especially for the high density case, and the data in a 0.6 nm wide window around the D_α line are disregarded. For the upper spectrum, the halo is very wide due to the high T_i and the beam attenuation is low, such that the MSE spectrum can be studied best. The red line is the fit to the data, and the contributions of full, half, and third energy component and the halo are also shown. For this line-of-sight, the angles are $\psi\approx84^0$ and $\phi\approx3^0$. For an ideal mirror we would expect equal areas under the central σ-peak and the sum of the two π-peaks. However, the σ-line is suppressed by about a factor of 2 since its polarisation direction nearly agrees with the p-polarisation direction of the deflecting mirror. The suppression is stronger than expected from the literature data for the index of refraction n for Rh. A variation of the complex part of n was performed until the minimum of χ^2 of the fit was found
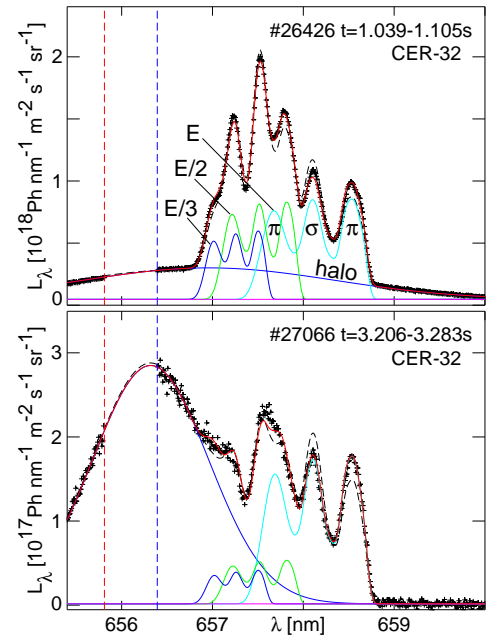
Fig.3: *Mesured Beam emission spectra and fit for #26426 with T_i=9.6 keV and n_e=2×10^{19} m^{-3} and #27066 with T_i=1.6 keV and n_e=1×10^{20} m^{-3}.*
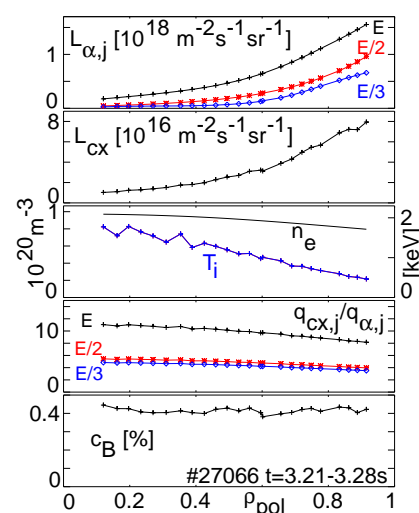
and yielded $\Im(n) = 4$. The fit with the nominal values for n has 5 time higher χ^2 and is shown as a dashed black line. Also for the lower spectrum of Fig.3, which is measured in a plasma with a 5 times higher density of $n_e=1\times10^{20}$ m^{-3}, the same suppression of the σ-line leads to the best fit. A measurement of the polarisation dependent mirror reflectivity is planned for after the experimental campaign. The MSE spectrum at high density is roughly a factor of 10 weaker and especially for the component with 1/3 energy, a good measurement of the beam halo contribution is important to obtain reliable information on the beam emission. Further improvements of the spectroscopic setup to minimise the influence of the strong passive D$_\alpha$ light on this part of the spectrum are required.

Evaluation of Impurity Densities

The D$_\alpha$ beam emission is proportional to the population of beam atoms excited to the n=3-level, which can be calculated with collisional-radiative models as provided by ADAS [1]. The radiance for the energy component j is: $L_{\alpha,j} = n_e q_{\alpha,j}(E_{b,j}, n_e, T_i, T_e, Z_{eff}) \int_{los} n_{b,j} dl$, where $q_{\alpha,j}$ is an effective photon emission coefficient depending on the beam energy and a number of plasma parameters. The plasma parameters shall be mean values for the line-of-sight volume inside the beam. For the active CX-emission of an impurity with concentration c_{imp}, we get a similar expression $L_{cx} = n_e c_{imp} \sum_j q_{cx,j} \int_{los} n_{b,j} dl$, where the effective CX photon emission coefficient $q_{cx,j}$ for energy component j includes the charge exchange from ground state and excited state beam atoms and also depends on the above plasma parameters. Thus the impurity concentration is given by: $c_{imp} = L_{cx}/\sum_j[L_{\alpha,j}q_{cx,j}/q_{\alpha,j}]$. The factor $q_{cx,j}/q_{\alpha,j}$ denotes the number of CX-photons per D$_\alpha$ photon for an impurity concentration of 1. Fig.4 shows an example for this evaluation for the boron concentration in the high density H-mode plasma #27066. Radial profiles for one beam blip are shown versus the normalised poloidal flux label ρ_{pol}. In the 1st box, the radiance of the D$_\alpha$ beam emission of all three energy components of the beam is depicted for the lines-of-sights of the CXRS diagnostic. The CXRS measurements used the n=7-6 transition of B^{4+} at λ=494.5 nm, whose radiance is shown in the 2nd box. The electron density in the 3rd box is

Fig.4: *Impurity concentrations from CXRS and beam emission spectroscopy for #27066.*

taken from unfolded interferometric measurements, while T_i is from CXRS. The dependence of the atomic data on T_e is very weak and we used $T_e = T_i$. The atomic factors $q_{cx,j}/q_{\alpha,j}$ in the 4th box were evaluated assuming $Z_{eff} = 1.6$. Most of the boron emission is due to the full energy component of the beam. The calculated boron concentration in the lowest box is very flat around 0.4%. This result still needs to be compared with beam attenuation calculations. Sensitivity tests to the used plasma parameters have to be done and the latest ADAS data revision [2] needs to be included. The beam excitation model can also be checked separately since the relation between $\int_{los} n_{b,j} dl$ and the total power in the beam is known from the beam model. At this high density, the excitation model must be about right since the calculated beam power at the outermost point is 2.4 MW which nicely compares with the nominal injected power of 2.56 MW.

References

[1] H.P. Summers, ADAS User Manual 2.6 (2004). http://www.adas.ac.uk./manual.php
[2] E. Delabie et al, Plasm. Phys. Control. Fusion **52**(2010)125008.